

# Correlation effects in bistability at the nanoscale: steady state and beyond

E. Khosravi,<sup>1,2</sup> A.-M. Uimonen,<sup>3,2</sup> A. Stan,<sup>3,2</sup> G. Stefanucci,<sup>4,5,2</sup>  
S. Kurth,<sup>6,7,2</sup> R. van Leeuwen,<sup>3,2</sup> and E. K. U. Gross<sup>1,2</sup>

<sup>1</sup>*Max-Planck Institut für Mikrostrukturphysik, Weinberg 2, D-06120 Halle, Germany*

<sup>2</sup>*European Theoretical Spectroscopy Facility (ETSF)*

<sup>3</sup>*Department of Physics, Nanoscience Center, FIN 40014, University of Jyväskylä, Jyväskylä, Finland*

<sup>4</sup>*Dipartimento di Fisica, Università di Roma Tor Vergata,*

*Via della Ricerca Scientifica 1, 00133 Rome, Italy*

<sup>5</sup>*INFN, Laboratori Nazionali di Frascati, Via E. Fermi 40, 00044 Frascati, Italy*

<sup>6</sup>*Nano-Bio Spectroscopy Group, Departamento de Física de Materiales,  
Universidad del País Vasco UPV/EHU, Centro Física de Materiales CSIC-UPV/EHU,  
Avenida de Tolosa 72, E-20018 San Sebastián, Spain*

<sup>7</sup>*IKERBASQUE, Basque Foundation for Science, E-48011 Bilbao, Spain*

(Dated: July 28, 2021)

The possibility of finding multistability in the density and current of an interacting nanoscale junction coupled to semi-infinite leads is studied at various levels of approximation. The system is driven out of equilibrium by an external bias and the non-equilibrium properties are determined by real-time propagation using both time-dependent density functional theory (TDDFT) and many-body perturbation theory (MBPT). In TDDFT the exchange-correlation effects are described within a recently proposed adiabatic local density approximation (ALDA). In MBPT the electron-electron interaction is incorporated in a many-body self-energy which is then approximated at the Hartree-Fock (HF), second-Born (2B) and *GW* level. Assuming the existence of a steady-state and solving directly the steady-state equations we find multiple solutions in the HF approximation and within the ALDA. In these cases we investigate if and how these solutions can be reached through time evolution and how to reversibly switch between them. We further show that for the same cases the inclusion of dynamical correlation effects suppresses bistability.

PACS numbers: 72.10.Bg,71.10.-w,31.15.xm,31.15.ee

## I. INTRODUCTION

The phenomenon of bistability has been the subject of several studies in the field of quantum transport. In their seminal paper Goldman *et al.*<sup>1</sup> reported the observation of bistability in the I-V curve of double-barrier resonant tunneling (DBRT) structures, thus stimulating many theoretical<sup>2-5</sup> and experimental investigations<sup>6,7</sup> on the subject. The bistability is a non-linear effect induced by the electrostatic charge build-up in the quantum well and occurs in the bias window of negative differential resistance.<sup>1</sup> From the theoretical point of view, various techniques have been used to capture this phenomenon, ranging from a crude estimate of the charge build-up<sup>6</sup> to self-consistent calculations at a mean field-level.<sup>2-4,8-10</sup>

With the increasing interest in transport through nanoscale devices, in particular using molecules as a possible component of future electronic circuits, the study of intrinsic bistability in nanoelectronics has gained new attention. The possibility of finding molecular devices equivalent to conventional non-linear devices, such as diodes and transistors, is indeed an attractive perspective. There have already been some successful attempts along these lines. Molecular devices with large on-off current ratio and large negative differential resistance, behaving similarly to mesoscopic DBRT structures, have been reported.<sup>11,12</sup> So far, the great majority of bistabil-

ity studies have been limited to the steady-state regime and performed within the framework of the Landauer formalism combined with static density functional theory (DFT). At the Hartree level, bistability was reported for a double quantum dot structure.<sup>13,14</sup> In the context of time-dependent (TD) DFT, the inclusion of memory effects beyond the adiabatic approximation is not straightforward and the development of accurate functionals to be used in numerical calculations is still under way. A promising and timely, even though computationally demanding, alternative is the solution of the Kadanoff-Baym (KB) equations<sup>15-21</sup> using self-energies from many-body perturbation theory (MBPT). The advantage of MBPT over TDDFT is the inclusion of dynamical exchange-correlation (XC) effects, i.e., effects arising from a frequency-dependent self-energy, in a more systematic way through the selection of suitable Feynman diagrams. Thus, MBPT provides an important tool to go beyond the commonly used adiabatic approximations and to quantify the importance of dynamical XC effects.

The fundamental issue which we address in this paper is whether the bistability phenomenon found in static DFT, Hartree and Hartree-Fock (HF) approximation survives when dynamical XC effects are taken into account. In contrast to DFT and mean-field approximations the steady-state equations of MBPT do not form a closed set of equations for the density only. This difficulty renders the search for the bistability regime in MBPT computationally very costly. To overcome the problem

we implement a time-dependent strategy.<sup>20–29,31–34</sup> We first solve the steady-state equations of DFT and mean-field theory to determine the parameter range for bistability. Then we go beyond the current state-of-the-art and provide a TD description of the bistability phenomenon in adiabatic TDDFT<sup>23–29</sup> and TD mean field theory. We show how to switch between different stable states by means of ultrafast gate voltages or external biases (driving fields). The possibility of reversibly switching between different stable steady-states is an aspect that has remained largely unexplored.<sup>30</sup> Knowing how to steer the electron dynamics in real time we use the same driving fields in correlated MBPT simulations. The calculations are performed with the fully self-consistent second-Born (2B) and *GW* approximations which have recently been shown<sup>31</sup> to agree with numerically exact TD-DMRG results.<sup>35</sup> In all cases studied here where adiabatic DFT and HF theory predict bistability *dynamical XC effects destroy the phenomenon*.

The paper is organized as follows: In Section II we introduce the model used in our study. In Section III we introduce the TDDFT approach to transport, with a particular emphasis on the real-time propagation to study time-dependent transport phenomena. Assuming that the system reaches a steady state, the steady-state density can be calculated without explicitly propagating in time, as explained in Section III B. In this Section a separate (fixed-point) analysis is given to determine whether or not a solution is stable. As an alternative real-time approach to transport, we introduce in Section IV the MBPT approach based on the solution of the KB equations. In Section V, we present the results of our numerical simulations for a certain set of parameters for which multiple solutions are observed in DFT. Finally, conclusions are drawn in Section VI.

## II. THE MODEL

In this work we study multistability in quantum transport, i.e., we study the question if, for a given set of parameters, a biased system can have more than one steady state. Apart from proposing a way to classify the different steady states as stable or unstable, we also investigate by explicit time evolution the possibility to reversibly switch between different steady states by application of a suitably chosen, time-dependent perturbation.

These questions are addressed in model systems. We consider a nanoscale device consisting of a few interacting sites contacted to two non-interacting tight-binding leads. Initially, the contacted system is in equilibrium at a given temperature and chemical potential. At time  $t_0 = 0$  we switch on a bias in the leads and follow the time evolution of the perturbed system.

The Hamiltonian of the system consists of three different parts

$$\hat{H}(t) = \hat{H}_C(t) + \sum_{\alpha=L,R} \hat{H}_\alpha(t) + \hat{H}_T, \quad (1)$$

where the Hamiltonian  $\hat{H}_C(t)$  of the central device describes a chain of  $N_C$  sites with a Hubbard-type on-site electron-electron interaction:

$$\begin{aligned} \hat{H}_C(t) = & \sum_{i=1}^{N_C} \varepsilon_i^C(t) \hat{d}_{i\sigma}^\dagger \hat{d}_{i\sigma} - \sum_{i=1}^{N_C-1} (V_C \hat{d}_{i\sigma}^\dagger \hat{d}_{i+1\sigma} + H.c.) \\ & + \frac{1}{2} \sum_{i=1}^{N_C} \sum_{\sigma\sigma'} U \hat{d}_{i\sigma}^\dagger \hat{d}_{i\sigma'}^\dagger \hat{d}_{i\sigma} \hat{d}_{i\sigma'}. \end{aligned} \quad (2)$$

Here,  $\hat{d}_{i\sigma}^\dagger$  ( $\hat{d}_{i\sigma}$ ) denote creation (annihilation) operators for electrons with spin  $\sigma$  at site  $i$ . The  $\varepsilon_i^C(t)$  are on-site energies which may consist of an arbitrary time-dependent part, denoted as  $V_{g,i}(t)$ , plus a time-independent part,  $\varepsilon_i^C$ . The nearest-neighbor hopping in the chain is  $V_C$  and  $U$  is the on-site Hubbard interaction.

The non-interacting left ( $L$ ) and right ( $R$ ) leads,  $\alpha = L, R$ , are described by one-dimensional semi-infinite chains with Hamiltonian

$$\begin{aligned} \hat{H}_\alpha(t) = & \sum_{i=1}^{\infty} (\varepsilon_\alpha + W_\alpha(t)) \hat{c}_{i\sigma\alpha}^\dagger \hat{c}_{i\sigma\alpha} \\ & - \sum_{i=1}^{\infty} (V_\alpha \hat{c}_{i\sigma\alpha}^\dagger \hat{c}_{i+1\sigma\alpha} + H.c.), \end{aligned} \quad (3)$$

with creation (annihilation) operators  $\hat{c}_{i\sigma\alpha}^\dagger$  ( $\hat{c}_{i\sigma\alpha}$ ) for electrons with spin  $\sigma$  at site  $i$  in the lead  $\alpha$ . The on-site energies  $\varepsilon_\alpha$  and the hopping matrix elements  $V_\alpha$  are independent of time and site index while  $W_\alpha(t)$  describes a time-dependent, site-independent bias applied to the lead  $\alpha$ .

Finally, the tunneling Hamiltonian which couples the leads to the device is given by

$$\hat{H}_T = - \sum_{\sigma} \left( V_{\text{link}} \hat{d}_{1\sigma}^\dagger \hat{c}_{1\sigma L} + V_{\text{link}} \hat{d}_{N_C\sigma}^\dagger \hat{c}_{1\sigma R} + H.c. \right), \quad (4)$$

where we have adopted the convention that the site in the lead  $\alpha$  connected to the device is labeled by the site index 1 and  $V_{\text{link}}$  is the hopping between the central region and the leads.

## III. MULTISTABILITY IN TIME-DEPENDENT DENSITY FUNCTIONAL THEORY

In this section we introduce the TDDFT approach<sup>40</sup> which we will use to investigate multistability in our model system. In TDDFT, the complicated problem of interacting electrons is mapped, in principle exactly, on the much simpler problem of non-interacting Kohn-Sham (KS) electrons moving in an effective local potential, thus providing a natural way to account for correlation effects in both leads and device region.<sup>23,25</sup> Since the method only involves the propagation of single-particle

wavefunctions, it promises for a computationally efficient way to study time-dependent phenomena in quantum transport.<sup>26</sup> The real-time TDDFT approach to transport will be described in Sec. III A. While in principle exact, in practice TDDFT requires the use of approximations for the time-dependent XC functionals. The most popular one, the adiabatic local density approximation (ALDA), depends only on the *local* and *instantaneous* density, i.e., it does not include memory effects. On one hand this feature is certainly a shortcoming of the approximation whose consequences for time-dependent transport still need to be explored. On the other hand, in the context of multistability, this approximation allows one to formulate the steady-state condition in terms of a closed set of non-linear equations for the steady-state density. The solution of these equations allows for an efficient scan of parameter space to find those parameter values for which multistability is possible. This steady-state approach with the local and adiabatic approximation of TDDFT will be described in Sec. III B.

### A. Real-time TDDFT for transport

One of the technical difficulties in applying TDDFT to quantum transport lies in the necessity of propagating an infinite non-periodic system, or equivalently, a finite open system attached to semi-infinite leads. Here we sketch the technique how this can be achieved. The technical details of the algorithm can be found in Ref. 26.

In a localized (site) basis, the KS Hamiltonian of the total system consisting of left lead, device, and right lead can be partitioned in a block-diagonal matrix form as

$$\begin{pmatrix} \mathbf{H}_{LL}^{KS}(t) & \mathbf{H}_{LC} & 0 \\ \mathbf{H}_{CL} & \mathbf{H}_{CC}^{KS}(t) & \mathbf{H}_{CR} \\ 0 & \mathbf{H}_{RC} & \mathbf{H}_{RR}^{KS}(t) \end{pmatrix}, \quad (5)$$

where  $\mathbf{H}_{CC}^{KS}(t)$  is the Hamiltonian of the isolated device and  $\mathbf{H}_{\alpha\alpha}^{KS}(t) = \mathbf{H}_{\alpha\alpha}^{KS} + \mathbf{W}_{\alpha}^{KS}(t)$  is the Hamiltonian of the isolated lead  $\alpha$ . The time-dependent potential in the leads has the simple form  $\mathbf{W}_{\alpha}^{KS}(t) = W_{\alpha}(t)\mathbb{1}_{\alpha}$  where  $\mathbb{1}_{\alpha}$  is the identity matrix for lead  $\alpha = L, R$ . Finally,  $\mathbf{H}_{C\alpha}$  and  $\mathbf{H}_{\alpha C}$  describe the coupling between lead  $\alpha$  and the device. Here and in the following we use boldface notation to indicate matrices in one-electron labels.

Using downfolding techniques one can derive the equation of motion for the  $k$ -th KS single-particle orbital projected onto the central region,  $\psi_{k,C}(t)$ , which reads

$$\begin{aligned} [i\partial_t - \mathbf{H}_{CC}^{KS}(t)] \psi_{k,C}(t) &= \int_0^t d\bar{t} \Sigma_{\text{em}}^R(t, \bar{t}) \psi_{k,C}(\bar{t}) \\ &+ \sum_{\alpha} \mathbf{H}_{C\alpha} \mathbf{g}_{\alpha\alpha}^R(t, 0) \psi_{k,\alpha}(0). \end{aligned} \quad (6)$$

Here,  $\psi_{k,\alpha}(0)$  is the projection of the  $k$ -th KS orbital on lead  $\alpha$  at the initial time  $t_0 = 0$ ,  $\mathbf{g}_{\alpha\alpha}^R(t, t')$  is the retarded Green function of the isolated lead  $\alpha$  and the retarded

embedding self-energy is defined as

$$\Sigma_{\text{em}}^R(t, t') = \sum_{\alpha=L,R} \mathbf{H}_{C\alpha} \mathbf{g}_{\alpha\alpha}^R(t, t') \mathbf{H}_{\alpha C}. \quad (7)$$

The time-dependent density at site  $j$  of region  $C$  at zero temperature can be written as

$$n_j(t) = 2 \sum_k^{\text{occ}} |\psi_{k,C}(j, t)|^2, \quad (8)$$

where the sum runs over the occupied KS orbitals and the prefactor is due to spin degeneracy.

In our model the KS Hamiltonian matrix  $\mathbf{H}_{CC}^{KS}(t)$  has a tridiagonal form where the only non-vanishing entries are the off-diagonal matrix elements  $[\mathbf{H}_{CC}^{KS}(t)]_{j,j+1} = [\mathbf{H}_{CC}^{KS}(t)]_{j+1,j} = -V_C$  with  $j = 1, \dots, N_C - 1$ , and the diagonal matrix elements

$$\begin{aligned} [\mathbf{H}_{CC}^{KS}(t)]_{jj} &= v_{\text{KS}}(j, t) \\ &= \varepsilon_j^C(t) + v_H[n_j(t)] + v_{\text{xc}}[n](j, t), \end{aligned} \quad (9)$$

with  $j = 1, \dots, N_C$ . The second term on the r.h.s of Eq. (9) is the Hartree potential and the third term is the XC potential of TDDFT for model systems.<sup>36,37</sup> Although in our model the interaction is restricted to the device region only, the exact XC potential has contributions in the adjacent lead regions as well and will rigorously vanish only deep inside the leads.<sup>38,39</sup> Therefore, already at this point we make an approximation by restricting the XC potential to the device region only.

Of course, the exact form of  $v_{\text{xc}}[n]$  is unknown and in practice one has to resort to approximations. For lattice systems, a local density approximation (LDA) based on the Bethe ansatz solution of the uniform one-dimensional Hubbard model has been suggested<sup>41,42</sup> and a parameterization of this Bethe ansatz LDA (BALDA) has been presented in Ref. 41. The adiabatic version<sup>43</sup> of this functional (ABALDA) makes  $v_{\text{xc}}[n]$  local in both space and time, i.e.,  $v_{\text{xc}}[n](j, t) = v_{\text{xc}}(n_j(t))$ . The original BALDA was designed for the uniform Hubbard model with Hubbard interaction  $U$  and nearest-neighbor hopping  $V$  everywhere. A modification of this functional for the case of a single interacting impurity site ( $N_C = 1$ ) connected by a hopping matrix element  $V_{\text{link}}$  to the leads with hopping  $V$  has been suggested in Ref. 45. In this work we use this modified functional both for the case of a single impurity<sup>31</sup> and also for  $N_C > 1$  where in the latter case we impose the restriction that the hopping  $V_C$  between the sites in the central region is equal to the hopping  $V_{\text{link}}$  from the chain to the leads. A particularly interesting property of the BALDA is its discontinuity at integer values of the occupation number.<sup>44</sup> This discontinuity has a fundamental impact for time-dependent transport in the Coulomb blockade regime and may prevent a biased system from evolving towards a steady state.<sup>45</sup>

Finally, we note that for our Hubbard-like form of the interaction, where each electron interacts only with electrons of opposite spin on the same site, also the HF potential becomes a local potential depending only on the local

density. In our numerical studies we will also present results obtained within the HF approximation.

### B. Adiabatic approximation: Steady-state condition for the density

Following the time evolution of the system as it is driven out of equilibrium by applying a bias in the leads, tells us if and how the system attains a steady state in the long-time limit. However, without doing the actual time propagation, we can also *assume* that the system approaches a steady state and study the consequences of this assumption. In the context of multistability in TDDFT, a particularly useful consequence is that, within the local and adiabatic approximation, it is possible to derive a self-consistency condition for the steady-state density.

Using non-equilibrium Green function techniques, the steady-state density  $\tilde{n}_j := \lim_{t \rightarrow \infty} n_j(t)$ , can be obtained from the lesser Green function projected onto the central region,  $\mathbf{G}_{CC}^<$ , as

$$\tilde{n}_j = 2 \int \frac{d\omega}{2\pi i} [\mathbf{G}_{CC}^<(\omega)]_{jj}. \quad (10)$$

The lesser Green function can, in turn, be obtained from

$$\mathbf{G}_{CC}^<(\omega) = \mathbf{G}_{CC}^R(\omega) \Sigma_{\text{em}}^<(\omega) \mathbf{G}_{CC}^A(\omega), \quad (11)$$

where  $\Sigma_{\text{em}}^<(\omega)$  is the lesser embedding self-energy while  $\mathbf{G}_{CC}^R = [\mathbf{G}_{CC}^A]^\dagger$  is the retarded KS Green function which, at the steady state, reads

$$\mathbf{G}_{CC}^R(\omega) = \left( \omega - \tilde{\mathbf{H}}_{CC}^{KS}(\tilde{n}) - \Sigma_{\text{em}}^R(\omega) \right)^{-1}. \quad (12)$$

In this formula

$$\tilde{\mathbf{H}}_{CC}^{KS}(\tilde{n}) := \lim_{t \rightarrow \infty} \mathbf{H}_{CC}^{KS}(t), \quad (13)$$

is the asymptotic value of the KS Hamiltonian in the central region. Note that  $\tilde{\mathbf{H}}_{CC}^{KS}$  depends on  $\tilde{n}$  only in the local and adiabatic approximation.

For the 1D tight-binding leads the retarded embedding self-energy has the structure

$$[\Sigma_{\text{em}}^R(\omega)]_{ij} = \Sigma_{\text{em},L}^R(\omega) \delta_{i,1} \delta_{j,1} + \Sigma_{\text{em},R}^R(\omega) \delta_{i,N_c} \delta_{j,N_c}, \quad (14)$$

and therefore the self-consistency condition (10) becomes

$$\tilde{n}_j = \int \frac{d\omega}{\pi} (f_L(\omega) \Gamma_L(\omega) |[\mathbf{G}_{CC}^R(\omega)]_{1,j}|^2 + f_R(\omega) \Gamma_R(\omega) |[\mathbf{G}_{CC}^R(\omega)]_{N_c,j}|^2), \quad (15)$$

with the shifted Fermi function  $f_\alpha(\omega) = f(\omega - \tilde{W}_\alpha)$  and  $\tilde{W}_\alpha := \lim_{t \rightarrow \infty} W_\alpha(t)$ . Since the KS Green function of Eq. (12) depends on  $\tilde{n}$  only, Eq. (15) is a set of coupled nonlinear equations for the steady-state density  $\tilde{n}_j$ ,  $j = 1, \dots, N_c$ , at the sites of the device region. Due to the

nonlinearity of these equations, more than one fixed point solutions may exist. Therefore, one can use Eq. (15) to scan the parameter space for possible multiple steady states. Once these values are identified we can investigate if and how the different steady states are attained by time propagation.

We close this Section by recalling a few basic properties of a fixed-point (FP) solution<sup>46</sup> which we will use in the following to interpret and understand our numerical results. Consider a system of  $N_C$  coupled equations of the following general form

$$\mathbf{n} = \mathbf{g}(\mathbf{n}), \quad \mathbf{n} = (n_1, n_2, \dots, n_{N_C}). \quad (16)$$

Let the vector  $\tilde{\mathbf{n}}$  be a fixed point solution of Eq. (16) and  $\mathbf{J}$  the Jacobian matrix  $\frac{d\mathbf{g}}{d\mathbf{n}}|_{\tilde{\mathbf{n}}}$ . A fixed point is stable if the modulus of all eigenvalues of  $\mathbf{J}$  is smaller than unity, partially unstable if there exist at least one eigenvalue with modulus larger than unity (saddle point), and it is totally unstable if the modulus of all eigenvalues is larger than unity.

## IV. MANY-BODY TECHNIQUE: KADANOFF-BAYM EQUATIONS

An alternative approach to TDDFT for transport is the time-dependent MBPT formulation of transport<sup>20,21</sup> based on the time evolution of the Green function via the KB equations.<sup>15-19</sup> In the MBPT, the many-body self-energy  $\Sigma_{\text{MB}}$  can be approximated by a selection of suitable Feynman diagrams, relevant for the description of the main scattering processes. In earlier work<sup>31</sup> we have found that the 2B approximation is in excellent agreement with accurate TD-DMRG results in the regime of weak to intermediate interaction strength for the Anderson impurity model.<sup>35</sup> Hence the 2B approximation is extremely useful for benchmarking other approximations. The main quantity of MBPT is the Keldysh Green function,  $\mathbf{G}(z, z')$ , where  $z$  and  $z'$  are time coordinates on the Keldysh contour  $\mathcal{C}$ .<sup>47-49</sup> To describe the electron dynamics of the system, the Keldysh Green function is propagated in time according to the KB equations. Since we are interested in the dynamical processes occurring in the central region, we can again use embedding techniques to derive the equation of motion for the Green function  $\mathbf{G}_{CC}$  projected on the central region. This equation reads

$$[i\partial_z - \mathbf{H}_{CC}(z)] \mathbf{G}_{CC}(z, z') = \delta(z, z') + \int_{\mathcal{C}} d\bar{z} [\Sigma_{\text{em}}(z, \bar{z}) + \Sigma_{\text{MB}}(z, \bar{z})] \mathbf{G}_{CC}(\bar{z}, z'), \quad (17)$$

where, in addition to the embedding self-energy  $\Sigma_{\text{em}}(z, \bar{z})$ , we also have included a many-body self-energy  $\Sigma_{\text{MB}}(z, \bar{z})[\mathbf{G}]$ . This latter quantity is a functional of the Green function and fulfills all basic conservation laws.<sup>50,51</sup> We consider only the central region to be interacting and the leads are effectively noninteracting.

Therefore the many-body self-energy has nonvanishing elements only for the central region, because the diagrammatic expansion starts and ends with an interaction line.<sup>20,21</sup>

Equation (17) is an exact equation for  $\mathbf{G}_{CC}$ , provided an exact expression for  $\Sigma_{\text{MB}}$  is inserted. Of course, for practical calculations the many-body self-energy must be approximated. In this paper we explicitly considered the following *conserving* approximations for the self-energy; the HF, 2B and *GW* approximations. Their diagrammatic representations are illustrated in Fig. 1. The implementation of Eq. (17) requires a transformation into equations for real times, known as KB equations, which are then solved by time propagation.<sup>16,20,21,52</sup> From the knowledge of the Green function any one-particle property of the system can be extracted. In particular, the time-dependent density can be obtained from the lesser Green function as

$$n_j(t) = -2i[\mathbf{G}_{CC}^<(t, t^+)]_{jj}. \quad (18)$$

In the correlated case there is no simplification such as Eq. (8) since there are no more well defined single-particle states. Also the current through lead  $\alpha$  can be expressed in terms of the Keldysh Green functions and reads<sup>20,21</sup>

$$\begin{aligned} I_\alpha(t) = & 2\text{Re} \left\{ \text{Tr}_C \left[ \int_{t_0}^t d\bar{t} [\mathbf{G}_{CC}^<(t, \bar{t}) \Sigma_{\text{em}, \alpha}^A(\bar{t}, t) \right. \right. \\ & + \int_{t_0}^t d\bar{t} \mathbf{G}_{CC}^R(t, \bar{t}) \Sigma_{\text{em}, \alpha}^<(\bar{t}, t) \\ & \left. \left. - i \int_0^\beta d\bar{\tau} \mathbf{G}_{CC}^\lceil(t, \bar{\tau}) \Sigma_{\text{em}, \alpha}^\lceil(\bar{\tau}, t) \right] \right\}. \quad (19) \end{aligned}$$

Besides the superscripts *A* (advanced), *R* (retarded) and *<* (lesser) we also introduced the superscripts  $\lceil$  and  $\rceil$  to denote the components with one time argument on the imaginary axis and the other on the real axis and vice versa.<sup>23,49</sup> The trace is taken over one-electron indices in the central region. Eq. (19) generalizes the Meir-Wingreen formula<sup>53</sup> as it includes initial many-body and embedding effects through the integral along the imaginary track of the contour (last term).

For the interpretation of the numerical results we found it useful to look at the TD spectral function defined according to

$$A(T, \omega) = -\text{Im} \text{Tr} \int \frac{d\tau}{\pi} e^{i\omega\tau} [\mathbf{G}^> - \mathbf{G}^<](T + \frac{\tau}{2}, T - \frac{\tau}{2}), \quad (20)$$

where  $\tau = t - t'$  is a relative time and  $T = (t + t')/2$  is an average time coordinate. In equilibrium, this function is independent of  $T$  and has peaks below the Fermi level at the electron removal energies and above the Fermi level at the electron addition energies. If the time-dependent external field becomes constant after some switching time, then also the spectral function becomes independent of  $T$  after some transient period and has peaks at the addition and removal energies of the *non-equilibrium* biased

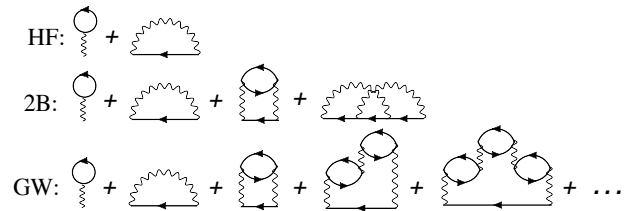


FIG. 1: Conserving many-body approximations.

system.

In the HF approximation the many-body self-energy is frequency independent and therefore the only broadening of the spectral peaks comes from the embedding part. This is also the case for the ABALDA. When going beyond the mean-field level, the self-energy becomes frequency dependent and as a consequence the peaks of the spectral function are typically broadened.

In the local and adiabatic approximation of TDDFT we have found a shortcut to determine if, for a given parameter set, the biased system can have multiple steady states (see Section IIIB). It is important to note that a similar shortcut does not exist in MBPT. The reason is that in MBPT the self-consistency condition for the steady-state density requires the knowledge of  $\mathbf{G}_{CC}(\omega)$  (to compute the many-body self-energy  $\Sigma_{\text{MB}}[\mathbf{G}_{CC}]$ ) and thus the equations cannot be closed in terms of the density only. As a consequence, in MBPT one does not have an efficient method to scan the parameter space to look for bistability. Although this feature is somewhat inconvenient for our analysis, physically it is quite reasonable because it implies that possible dynamical XC effects (arising from the frequency dependence of the many-body self-energy) are included.

## V. RESULTS

In this Section, we present the results of our numerical simulation for a certain set of parameters for which the self-consistency condition (15) admits multiple solutions. We investigate how one can switch between different stable solutions by applying a time-dependent gate voltage. We also demonstrate that for the same parameter sets the bistability is suppressed in the correlated many-body approximations, e.g., 2B and *GW*. The analysis will be carried out in two types of model devices, namely the one and two-site Hubbard models.

### A. Single site Hubbard model

As a first example, we study a single-site Hubbard model connected to semi-infinite leads with the following parameters:  $V_{\text{in}k} = 0.3$ ,  $W_L = 1.8$ ,  $W_R = -1.0$ ,  $U = 2.0$ ,  $\varepsilon^C = -0.6$ ,  $\varepsilon_\alpha = \varepsilon_F = 0$  (half-filled leads), and the

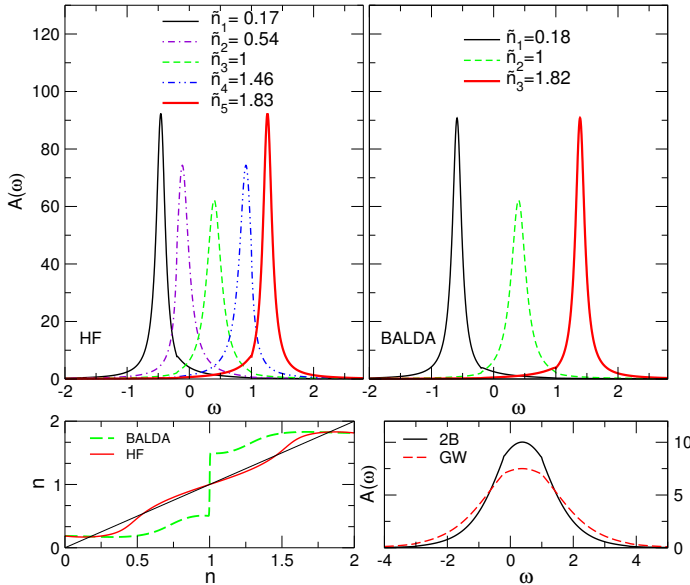


FIG. 2: Spectral functions for the different steady-state solution of the HF approximation (top-left panel) and BALDA (top-right panel). The graphical solution of Eq. (15) is displayed in the bottom-left panel for the HF and BALDA. For comparison we also report the 2B and *GW* steady-state spectral functions in the bottom-right panel.

inverse temperature  $\beta = 90$ . All energies are measured in units of the lead-hopping parameter  $V$ . In the biased system the band-width of the leads extends from  $\varepsilon_F + W_\alpha - 2V$  to  $\varepsilon_F + W_\alpha + 2V$ . With these parameters the self-consistent equation (15) admits five (three) solutions within the HF(BALDA) approximation. The fixed points are shown in the lower left corner of Fig. 2 where we display the left and right hand side of Eq. (15). The corresponding densities for the HF are  $\tilde{n}_1 = 0.17$ ,  $\tilde{n}_2 = 0.54$ ,  $\tilde{n}_3 = 1.0$ ,  $\tilde{n}_4 = 1.46$  and  $\tilde{n}_5 = 1.83$  while for the BALDA the three fixed point densities are  $\tilde{n}_1 = 0.18$ ,  $\tilde{n}_2 = 1.00$ ,  $\tilde{n}_3 = 1.82$ .

For a single site the fixed point theorem tells us that a solution is stable if  $|\frac{dg}{dn}| < 1$ , with  $g$  being the right-hand side of Eq. (15). Hence, one can see from Fig. 2 that the fixed points  $\tilde{n}_1$ ,  $\tilde{n}_3$  and  $\tilde{n}_5$  are stable in the case of the HF, while in case of the BALDA the stable solutions are  $\tilde{n}_1$  and  $\tilde{n}_3$ . Although the solution with density of unity exists for both approximations, it is stable in the HF approximation and unstable in the BALDA. In the upper panels of Fig. 2 we plot the steady-state spectral functions corresponding to the fixed points of the HF and BALDA. The HF peak for density  $\tilde{n}_1 = 0.17$  (and the BALDA peak for density  $\tilde{n}_1 = 0.18$ ) is located within the right lead energy continuum, while the HF peak for density  $\tilde{n}_5 = 1.83$  (and the BALDA peak for density  $\tilde{n}_3 = 1.82$ ) is located within the left lead energy continuum. By contrast, the HF spectral function of the unstable fixed points,  $\tilde{n}_2$  and  $\tilde{n}_4$ , are peaked at the edges of left and right lead band respectively. The HF and

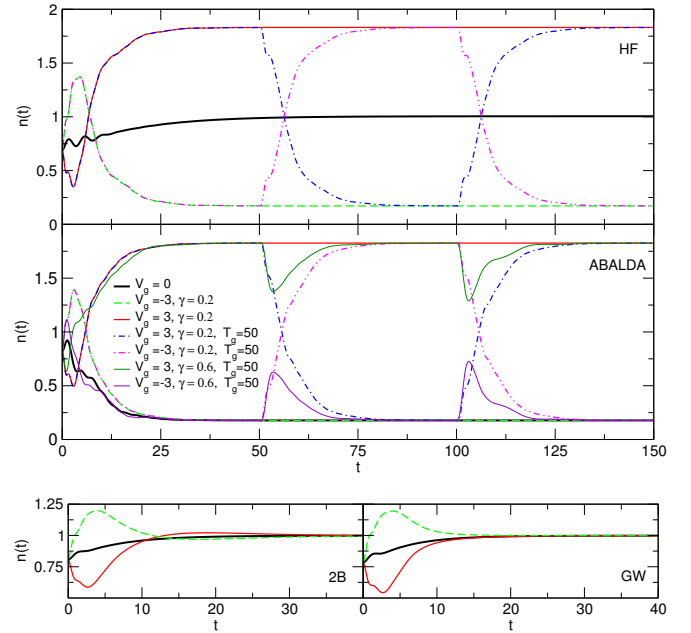


FIG. 3: Top panel: Time-dependent density in the HF approximation (top) and ABALDA (bottom) after the sudden switch on of the bias voltage and a series of gate pulses as in Eq. (21). Bottom panel: Time-dependent density within 2B (left) and *GW* approximations (right) after the sudden switch on of the bias voltage and a gate pulse as in Eq. (21) with  $V_g = -3, 0, 3$ .

BALDA spectral functions of the fixed point with density of unity are identical (the XC potential is zero in this case) and the peak is located exactly in the middle of the overlapping region between the left and right bands. In spite of this the stability condition of this fixed point is completely different in the HF and BALDA case. Since the multistability can be most easily observed if the spectral peaks of the stable solutions are well separated, we conclude that this phenomenon is favoured when the energy bands have a small overlap and the system is in the negative differential resistance (NDR) regime. As we shall see below, for the correlated MBPT approximations the situation is very different. In the lower left panel of Fig. 2 we show the 2B and *GW* steady-state spectral functions, as obtained from the propagation of the KB equations. The spectral weight is spread over the whole lead energy range and beyond. Consequently, the height of the spectral function is also much smaller. The considerable broadening is due to an increased quasi-particle scattering in the out of equilibrium system as already observed in Ref. 21.

Let us now study how to switch between different stable steady-state densities using ultrafast time-dependent driving fields. We start from the initially unbiased equilibrium system with ground-state density  $\tilde{n}_0 = 0.69$  ( $\tilde{n}_0 = 0.82$ ) for HF (BALDA). In Fig. 3 we show the time evolution of the density at the interacting site for different approximations after the sudden switch on of

the bias voltage  $W_L = 1.8$  and  $W_R = -1.0$ . In the HF approximation we observe that after some transient time the density approaches the value 1. The behavior of the ABALDA density is very different, in agreement with the fact that the solution with density of unity is unstable and hence cannot be reached by time evolution. At the steady state the ABALDA density equals the lowest value  $\tilde{n}_1$ .

To switch to the other stable solutions in real time we applied a time-dependent gate pulse on the Hubbard site. In this work we have used an exponentially decaying gate voltage of the form

$$V_g(t) = \begin{cases} V_g e^{-\gamma t} & , \text{ if } 0 < t < T_g \\ -V_g e^{-\gamma(t-T_g)} & , \text{ if } T_g < t < 2T_g \\ V_g e^{-\gamma(t-2T_g)} & , \text{ if } t > 2T_g \end{cases} \quad (21)$$

In Fig. 3 we show that in the HF case, the state with the lowest density  $\tilde{n}_1$  can be obtained (in addition to applying a sudden bias in the leads) by switching on a pulse with amplitude  $V_g = -3.0$ , decay rate  $\gamma = 0.2$  and  $T_g = \infty$ . The state with highest density  $\tilde{n}_5 = 1.83$  can be obtained in a similar fashion but now applying a gate with positive amplitude  $V_g = 3.0$ . Thus, by changing the amplitude of the gate voltage we can switch between stable steady-state solutions. For instance, with a first pulse of positive amplitude and  $T_g = 50 \gg 1/\gamma$  the system reaches the state with  $\tilde{n}_5$ . At the time  $T_g$  we apply a second pulse but with negative amplitude. The density shows a transient behavior after which it approaches the value  $\tilde{n}_1$ . If we now apply a third pulse of positive amplitude at time  $2T_g$  the density goes back to the initial value  $\tilde{n}_5$ . This is nicely illustrated in Fig. 3. In Fig. 4 we show the non-equilibrium HF spectral function  $A(T, \omega)$  of Eq. (20) for a double switch with  $V_g = -3.0$ ,  $\gamma = 0.2$  and  $T_g = 50$ . The figure enlightens an interesting aspect regarding the transition from one steady-state to another. The density rises from the lowest  $\tilde{n}_1$  to the highest  $\tilde{n}_5$  lingering for a while in the middle stable solution  $\tilde{n}_3$ .

Going back to Fig. 3 we see that also in the ABALDA the state with highest density  $\tilde{n}_3 = 1.83$  is reached by applying a gate pulse with  $V_g = 3.0$  and  $\gamma = 0.2$  (in addition to a sudden bias in the leads). If the amplitude is negative instead ( $V_g = -3.0$ ) the density increases first but eventually drops down and goes back to its initial value  $\tilde{n}_1$ . Like in the HF case we can switch back and forth between stable solutions by changing the sign of  $V_g$ . Not unexpectedly, however, the decay time  $\tau_\gamma \sim 1/\gamma$  cannot be arbitrarily short. If  $\tau_\gamma$  is too short the system does not have time to accumulate or lose enough density to change the self-consistent potential and after some transient it falls back to the previous steady-state value. This is clearly shown in Fig. 3 for the amplitude  $V_g = \pm 3.0$ ,  $T_g = 50$  and a faster decay rate  $\gamma = 0.6$ .

Intuitively one would expect that by increasing (decreasing) the on-site energy of the Hubbard site the density decreases (increases). However, the highest (lowest) stable steady-state density is obtained with a positive

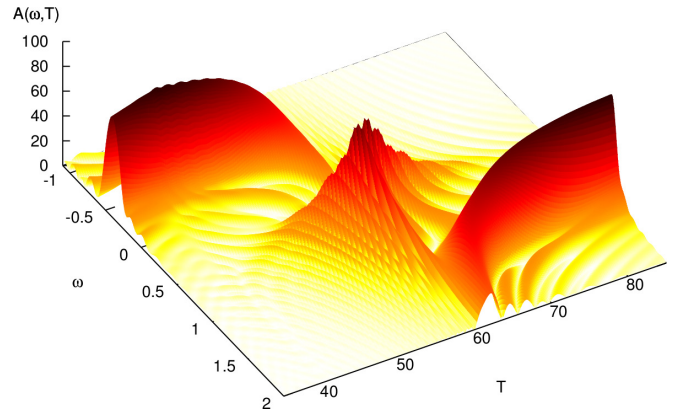


FIG. 4: Non-equilibrium spectral function for a gate pulse  $V_g = -3$ ,  $\gamma = 0.2$  which brings the density to  $\tilde{n}_1$  first, followed by a second identical gate pulse gate but with opposite amplitude which brings the density to  $\tilde{n}_5$ . The intermediate transition to the  $\tilde{n}_3$  stable solution is clearly visible.

(negative) gate. This is due to the fact that in our case the on-site energy of the Hubbard site lies below the energy band of the left lead. By applying a positive gate a finite hybridization occurs, leading to the migration of extra charge from the left lead to the Hubbard site. A similar argument explains the reduction of the density on the impurity site when a negative gate is turned on.

In the lower panels of Fig. 3 we plot the densities obtained within the 2B and  $GW$  self-energy approximations. We applied the bias voltage and a gate pulse of the form  $V_g(t) = V_g e^{-\gamma t}$  for  $t > 0$  with  $V_g = 0, \pm 3$ . In all cases only one steady state emerges at the end of the propagation with a density of about 1.0. It is worth observing that the 2B and  $GW$  steady-state values of the densities are close to each other, indicating that the single-bubble diagram, common to both approximations, is the dominant term of the perturbative expansion in this case.<sup>21</sup>

By time propagation we have shown that the three HF densities,  $\tilde{n}_1$ ,  $\tilde{n}_3$  and  $\tilde{n}_5$ , and the two ABALDA densities,  $\tilde{n}_1$  and  $\tilde{n}_3$ , are stable in a slightly different sense than that of the fixed point theorem. The fixed point theorem does not contain any information on the actual dynamics. Similarly, the HF solutions  $\tilde{n}_2$  and  $\tilde{n}_4$  as well as the ABALDA solution  $\tilde{n}_2$  are unstable in the sense that there exist no external perturbation to drive the system toward them. Thus, the fixed point theorem provides us with a good criterion to establish whether a given steady-state can be reached or not. This criterion is certainly rigorous in the limit of adiabatic switchings but, as we just found, its validity extends well beyond the adiabatic regime.

The time-dependent currents for the various approximations are shown in Fig. 5. Corresponding to the three stable HF steady-state densities there exist only two distinguishable values for the current  $I_R(t)$  at the interface between the Hubbard site and the right lead. The lower value corresponds to the solutions  $\tilde{n}_1$  and  $\tilde{n}_5$ , while the



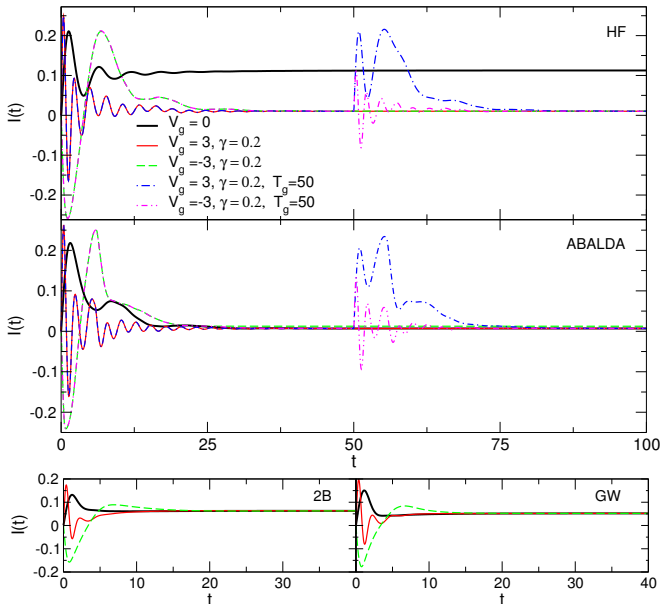


FIG. 5: Time-dependent current after the sudden switch on of the bias voltage and of a gate pulse as in Eq. (21) in the HF (top-upper panel), ABALDA (top-lower panel), 2B (bottom-left panel) and *GW* (bottom-right panel) approximations. In the HF and ABALDA case a time-dependent switch between two different steady-states is shown.

higher value corresponds to the solution  $\tilde{n}_3$ . The existence of only two solutions for the current is the consequence of an approximate particle-hole symmetry of the self-consistent equation (15), i.e.,  $\tilde{n}_5 \sim 1 - \tilde{n}_1$ . One particular appealing feature of the HF currents is the large difference between the two steady-state values, a highly desirable property for designing nanoscale diodes.

The particle-hole symmetry holds also for the ABALDA and therefore the steady-state currents corresponding to the two stable solutions are almost indistinguishable. Finally, the 2B and *GW* steady-state values of the currents, approach the same value independent of the gate voltage, in agreement with the existence of a unique steady state.

Increasing the bias the number of HF fixed point solutions reduces to three of which only two are stable. Also by increasing the interaction strength  $U$  the number of stable solutions reduces to two because a small amount of density causes a considerable change in the effective potential. Consequently, the middle solution becomes unstable.

## B. Two site Hubbard model

In this Section we consider the case of two interacting sites ( $N_C = 2$ ) connected to two semi-infinite, non-interacting tight-binding leads. We choose the following parameters:  $V_{\text{link}} = 0.4$ ,  $W_L = 2.2$ ,  $W_R = -1.2$ ,  $U = 2.0$ ,  $V_C = V_{1,2} = 0.4$ ,  $\varepsilon_\alpha = \varepsilon_F = 0$ ,  $\varepsilon_1^C = \varepsilon_2^C = -0.6$  and  $\beta =$

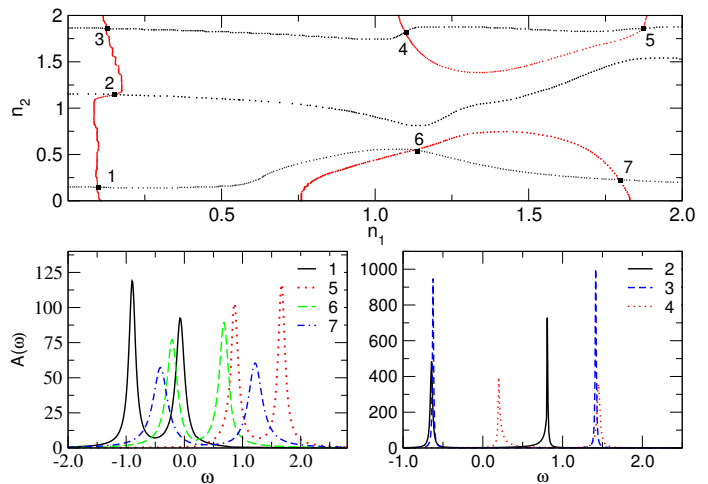


FIG. 6: Upper panel: Graphical solution of the integral in Eq. (15). Lower panel: Spectral functions for the HF approximation with Hubbard interactions corresponding to the seven different steady-state solutions for the density.

FP	$n_1$	$n_2$	FP	$n_1$	$n_2$
1	0.094	0.144	5	1.867	1.862
2	0.150	1.146	6	1.129	0.546
3	0.124	1.860	7	1.794	0.226
4	1.098	1.821			

TABLE I: Fixed point (FP) solutions of Eq. (15) for the steady-state densities of two interacting Hubbard sites connected to two biased, non-interacting leads in the HF approximation (see upper panel of Fig. 6). The parameters are:  $V_{\text{link}} = 0.4$ ,  $W_L = 2.2$ ,  $W_R = -1.2$ ,  $U = 2.0$ ,  $V_{1,2} = 0.4$ ,  $\varepsilon_\alpha = \varepsilon_F = 0$ , and  $\varepsilon_1^C = \varepsilon_2^C = -0.6$ .

90. The leads are half-filled and the lead bands have an energy range between  $\varepsilon_\alpha + W_\alpha - 2V$  and  $\varepsilon_\alpha + W_\alpha + 2V$ .

Within the HF approximation, the steady-state condition (15) then has seven solutions which are shown in the upper panel of Fig. 6. The black curve is obtained by finding the root of the equation  $n_2 - g_2(n_1, n_2) = 0$  at fixed  $n_1$  where  $g_2(n_1, n_2)$  is the right hand side of Eq. (15) with  $j = 2$ . The red curve is obtained in an analogous way by exchanging  $1 \leftrightarrow 2$ . Hence the intersections of the curves are the fixed points. The numerical values for the steady-state densities at the two Hubbard sites for the seven fixed points are given in Table I.

In the lower panel of Fig. 6 we show the spectral functions corresponding to the seven different fixed points (FP's). The spectral function for FP 1 is located mostly in an energy range within the energy band of the right lead, while the one for FP 5 has most of its weight in the energy range of the left lead. In contrast, FP's 6 and 7 have considerable weight in the energy bands of both leads. The spectral functions corresponding to FP's 2, 3, and 4 have much narrower peaks than the spectral functions for the other fixed points.

According to the fixed point theorem only the FP's 1, 3, 5, and 7 are stable and we expect them to be accessi-



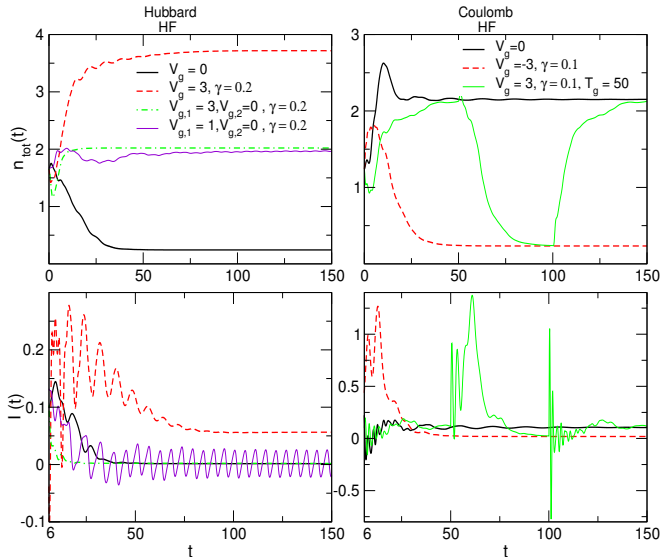


FIG. 7: Densities and currents for the HF approximation in case of short range (Hubbard) and long range (Coulomb) interactions. A switch between different steady-states by applying exponentially decaying gate of Eq. ((21)) are shown.

ble by time propagation. In the upper left panel of Fig. 7 we show the time evolution of the total density on the two dots,  $n_{\text{tot}}(t) = n_1(t) + n_2(t)$ , in the HF approximation for a sudden switch-on of the bias and several gate voltages starting from the equilibrium state with ground state density  $n_1 = n_2 = 0.83$ . The steady state corresponding to FP 1 is obtained by applying only the bias (no gate). In the case where we apply, in addition to the bias, a decaying gate voltage of the form (21) to both sites with  $V_{g,1} = V_{g,2} = V_g = 3.0$  and decay rate  $\gamma = 0.2$ , the total density increases and after some transient evolves towards the steady state corresponding to FP 5. In this case, lifting the on-site energy due to the gate voltage allows for extra charge to accumulate at the interacting sites such that the high-density steady-state solution can be achieved. In contrast, the solution of FP 7 can be obtained by applying the decaying gate voltage to the first (left) site only with amplitude  $V_{g,1} = 3.0$ ,  $V_{g,2} = 0$  and  $\gamma = 0.2$ .

Surprisingly, applying a similar asymmetric gate voltage but with a smaller amplitude ( $V_{g,1} = 1.0$ ,  $V_{g,2} = 0$ ), leads to a very different long time behavior. In this case the system does not evolve towards a steady state after the transients, instead we observe an oscillatory time-dependent density. In the long-time limit, the time-dependent total density (purple curve in the upper left panel of Fig. 7) oscillates with an amplitude of the order of  $10^{-3}$ , around 1.96. This value corresponds approximately to the total steady-state density of FP 3 of Fig. 6.

Despite this apparent similarity, the nature of these solutions is very different. While for the steady state of FP 7 the charge is mostly located at the first site, in the case of FP 3 the density on the first site is smaller than

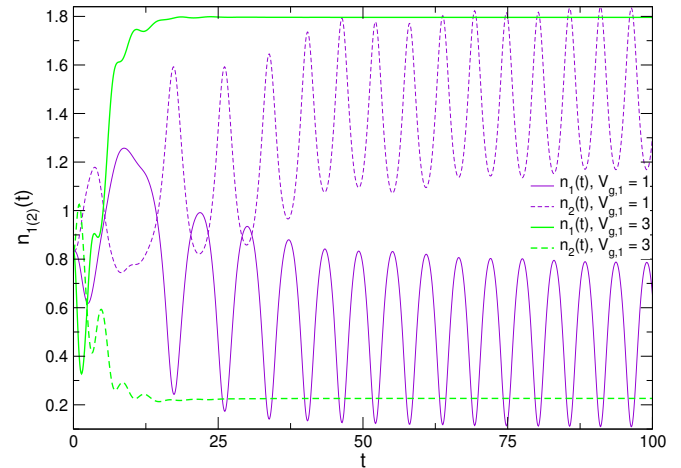


FIG. 8: Densities of the first and second site for the HF approximation in case of Hubbard interactions corresponding to the middle curves in the upper left panel of Fig. 7

on the second one (see Table I). The different nature of these two cases becomes even more obvious when looking at the time evolution of the density at the two interacting sites separately (see Fig. 8). While in the first case ( $V_{g,1} = 3.0$ ,  $V_{g,2} = 0$ ) the steady state is attained quite rapidly, in the second case ( $V_{g,1} = 1.0$ ,  $V_{g,2} = 0$ ) we see non-decaying density oscillations at the individual sites with rather large amplitudes. In the long-time limit the density oscillates thus inducing an oscillating KS potential. The persistence of these oscillations means that the density solves the Floquet system of equations in which the harmonics of the potential depend on the density itself. At first sight one might be reminded of non-decaying density and current oscillations which can appear for non-interacting systems when the biased system possesses two or more bound states. However, here we work in the HF approximation and therefore the analysis of Refs. 54–56 needs to be modified, see below.

Some insight into the nature of these oscillations can be gained from the simple model of an *isolated* Hubbard dimer. In the HF approximation, the equation of motion for the electronic density matrix  $\rho$  of the isolated dimer reads

$$i\partial_t \rho(t) = [H_{HF}(t), \rho(t)], \quad (22)$$

where the HF Hamiltonian is given by

$$H_{HF}(t) = \begin{pmatrix} \varepsilon_1 + U n_1/2 & V_{1,2} \\ V_{1,2} & \varepsilon_2 + U n_2/2 \end{pmatrix}. \quad (23)$$

Under the simplifying assumption  $\varepsilon_1 = \varepsilon_2$  one can then derive the equation of motion for the quantity  $\delta n(t) = n_1(t) - n_2(t) = \rho_{11}(t) - \rho_{22}(t)$  which reads

$$\delta \ddot{n} + (4V_{1,2}^2 - UD)\delta n + \frac{U^2}{8}(\delta n)^3 = 0, \quad (24)$$

where the constant  $D$  is related to the initial condition of Eq. (23) and can be defined through the off-diagonal

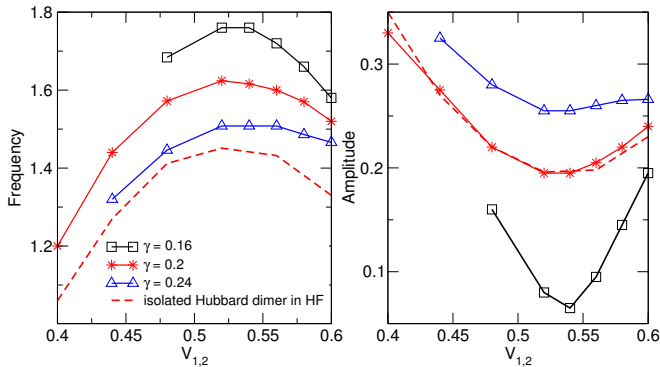


FIG. 9: Oscillation frequency and amplitude of the density oscillations found in HF for certain gate switchings of the Hubbard dimer connected to biased leads as function of the hopping between the Hubbard sites. For comparison, oscillation frequencies and amplitudes are given for the isolated Hubbard dimer in HF approximation described by Eq. (24).

matrix elements of the density matrix as

$$D = V_{1,2}(\rho_{1,2}(0) + \rho_{2,1}(0)) + \frac{U}{8}(\delta n(0))^2. \quad (25)$$

We note that Eq. (24) is the equation of motion of a classical, anharmonic oscillator and therefore supports oscillating solutions. We now check if the model of the isolated Hubbard dimer has anything to do with the oscillations seen in our transport setup. To this end, we calculate  $D$  from Eq. (24), i.e.,  $D = \frac{\delta \dot{n}}{\delta n U} + \frac{4V_{1,2}^2}{U} + \frac{U}{8}(\delta n)^2$ , where the densities and their time-derivatives are taken from the transport calculation after the transients have died out. As the Eq. (24) is an approximation for the connected Hubbard dimer,  $D$  is not constant in time. Hence in order to compare the oscillation amplitudes and frequencies from the transport simulations with those resulting from Eq. (24) we averaged  $D$  over an oscillation period. In Fig. 9 we show the dependence of oscillation frequency and amplitude for different switchings of the gate ( $V_{g,1}(t) = V_0 \exp(-\gamma t)$ ,  $V_{g,2}(t) = 0$ ,  $V_0 = 1$ ) as function of the hopping  $V_{1,2}$  between the two sites of the Hubbard dimer connected to biased leads and compare to the corresponding solutions of Eq. (24). We see that both frequency and amplitude of the isolated and connected dimer behave qualitatively quite similar as function of the intersite hopping and we conclude that the model of the isolated dimer certainly captures the physics behind these oscillations. We also would like to point out that the regions of parameter space where the oscillations are found appears to be quite small. For most parameters the system actually does evolve towards one of the steady states of Table I.

The occurrence of self-induced persistent oscillations in the HF mean field theory is favoured by the short-range nature of the Hubbard interaction. In fact, we also have studied a modified version of our model where we replaced the last term of Eq. (2) by a more long-range,

FP	$n_1$	$n_2$	FP	$n_1$	$n_2$
1	0.147	1.685	4	1.585	0.674
2	0.632	1.658	5	1.624	0.250
3	1.506	1.466			

TABLE II: Fixed point (FP) solutions of Eq. (15) for the steady-state densities of two interacting Hubbard sites connected to two biased, non-interacting leads in the BALDA approximation (see upper panel of Fig. 11). The parameters are:  $V_{\text{link}} = 0.4$ ,  $W_L = 2.2$ ,  $W_R = -1.2$ ,  $U = 2.0$ ,  $V_{1,2} = 0.4$ ,  $\varepsilon_\alpha = \varepsilon_F = 0$ , and  $\varepsilon_1^C = -0.04$ ,  $\varepsilon_2^C = 0.2$ .

Coulomb-like interaction  $\frac{1}{2} \sum_{\sigma\sigma'}^{i=1} U_{i,j} \hat{d}_{i\sigma}^\dagger \hat{d}_{j\sigma'}^\dagger \hat{d}_{j\sigma'} \hat{d}_{i\sigma}$  with

$$U_{i,j} = \begin{cases} U & i = j \\ \frac{U}{2|i-j|} & i \neq j \end{cases}. \quad (26)$$

In this case we have not found any oscillating solutions in the long-time limit. We have found two stable steady-state solutions accessible by time propagation. The first steady-state solution has densities  $n_1 = 1.06$ ,  $n_2 = 1.09$ , the second one has  $n_1 = 0.11$ ,  $n_2 = 0.13$ . The spectral functions corresponding to these solutions (see Fig. 10) are localized around the Fermi-level of the left or right lead respectively. The inclusion of the long range interaction destroys the states where the first peak is localized on the right lead energy band and the second peak is localized to the left lead energy band. Because the magnitude of the interaction felt by the electron on the site is now higher the density on the sites is decreased and the solution corresponding to the highest density is at half-filling. Also in this case we are able to switch between the two steady-states. The currents corresponding to these two solutions for the density have almost the same magnitude.

In Fig. 10 we show the time-dependent densities and currents for the 2B approximation. Again within the correlated approximations we find only one solution for the density and current. In the lower panels of Fig. 10 we show the spectral functions for the 2B and  $GW$  approximations compared to the spectral functions of the HF approximation. The 2B and  $GW$  spectral functions are qualitatively quite different from those of the HF approximation. Instead of the two peak structure of HF approximation, with 2B and  $GW$  approximations we have one very broad peak with much lower maximum.

We also studied the possibility of multiple steady-states for the same model within the BALDA. Using the same parameters as above, the BALDA has multiple solutions. However, at least one fixed point has a density on one of the dots very close to unity, exactly where the BALDA potential is discontinuous. For a single interacting dot, this discontinuity has been shown to be closely related to the Coulomb blockade phenomenon.<sup>45</sup> For the purposes of the present work we avoid the regime of integer occupancy in an ABALDA treatment by changing the on-site energies of the interacting sites in an asymmetric way such that  $\varepsilon_1^C = -0.04$  and  $\varepsilon_2^C = 0.2$ . With

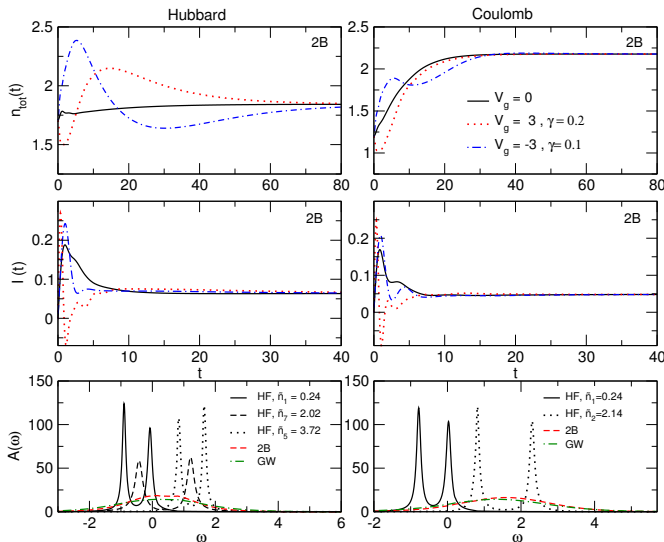


FIG. 10: Densities and currents for the 2B approximation short range (Hubbard) and long range (Coulomb) interactions are used. *Lower panel:* Spectral functions for the different approximations at the end of the time propagation.

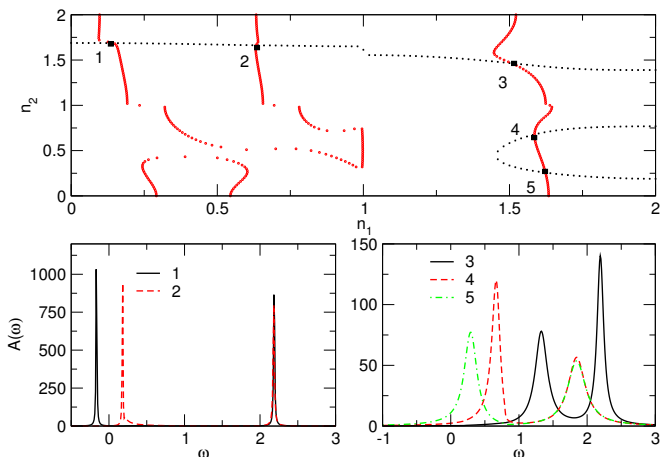


FIG. 11: Upper panel: Graphical solution of the integral in Eq. (15). Lower panel: Spectral functions for the BALDA with Hubbard interactions corresponding to the five different steady-state solutions for the density.

these modifications, the two coupled equations given by Eq. (15), are solved simultaneously, yielding five fixed-points (see Fig. 11 and Table II). Among these five fixed points, FP 1, FP 3, and FP 5 are stable, the other two unstable.

The spectral functions corresponding to FP 3 and FP 5 have two well separated smooth peaks, while the one corresponding to FP 1 has two sharp peaks, the first one located at  $\omega_1 = -0.168$  outside the energy range of the left lead, the second one at  $\omega_2 = 2.16$  outside the energy range of the right lead.

Again, the stable solutions are accessible by time propagation. Upon application of a sudden bias in the leads

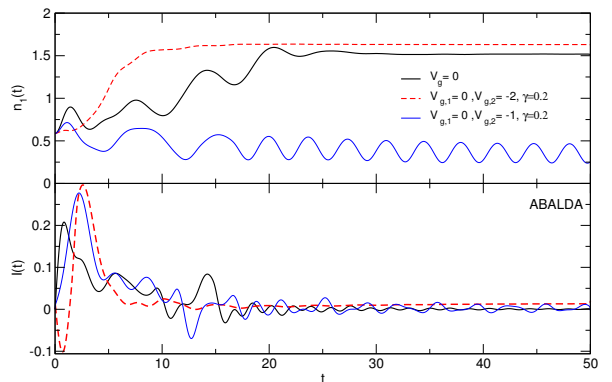


FIG. 12: Time-dependent density and current for the ABALDA with different applied gates.

at  $t = 0$ , the system approaches the third solution if no external gate voltage is turned on. On the other hand, if a gate voltage of the form (21) is applied only to the second site, with amplitude  $V_{g,2} = -2.0$  and  $\gamma = 0.2$ , the system attains a steady-state with a density corresponding to FP 5. As before switching between these two steady-state density is possible by changing the sign of the applied gate. A similar gate voltage applied only to the second site and smaller amplitude ( $V_g = -1.0$ ) leads to an oscillatory time-dependent density, whose average total density is close to the one of FP 1.

The frequency of the time-dependent density is  $\omega = 2.24$  which is close to the energy difference ( $\omega = 2.34$ ) between the peaks of spectral function. Hence, these oscillations are due to the existence of bound-states in the biased interacting system. One possible way to explain the role of bound-states in the biased KS Hamiltonian is that in the long-time limit the KS potentials are time dependent (with the bound state eigenenergy differences as prominent frequencies) leading again to time-dependent currents and densities (by virtue of Floquet's theorem). This is evidently achieved in adiabatic approximations with the XC potential depending only on the local density such as the ABALDA and HF approximation.

## VI. CONCLUSIONS

In this paper we have investigated by means of real-time propagation within MBPT and TDDFT, the existence of multiple steady states in single and double interacting quantum dot systems connected to semi-infinite leads. Within the framework of MBPT one can solve the steady-state MBPT equation without necessarily going through the whole time propagation. This can be done, by an iterative procedure like in Ref. 57, for example. In this case, starting from different initial guesses for the Green function, bistability would manifest itself in the convergence to more than one self-consistent solution. The advantage of the KB equations over the steady-state MBPT equations is that during the transient regime the

Green function explore a finite portion of the domain of all possible Green functions. Thus a single time propagation is similar to iteratively solving the steady-state MBPT equations for a large number of initial guesses.

In order to find the parameter region for bistability we first solved the self-consistent steady-state equations within the HF and BALDA approximation and determined the regime for which multiple solutions occur. We show that only the stable solutions are accessible by time propagation. Moreover, we find that by superimposing an exponentially decaying gate voltage pulse to the external bias, it is possible to reach the various stable solutions and also to switch between them. For the same parameters and driving fields, we then included dynamical XC effects by solving the Kadanoff-Baym equations with MBPT self-energies at the 2B and *GW* level of approximation. In all studied cases where adiabatic DFT and HF theory predict bistability *dynamical XC effects destroy the phenomenon*. Here we emphasize that we have performed 2B and *GW* calculations for many more parameter sets than those for which we have shown results in the present work. We have found no indication for the existence of multiple steady states for any of these sets. However, due to the vastness of the parameter space, we cannot rule out completely the possibility of multiple steady states when dynamical XC effects are included.

We wish to point out that even though ABALDA already contains correlations it is based on two approximations: the local and the adiabatic one. For any non-local

but adiabatic approximation to the TDDFT functionals one could still derive a self-consistency condition for the steady-state density in the form of coupled, nonlinear equations. Because of this nonlinearity multiple solutions, i.e., multiple steady states, can be possible. Therefore our results suggest that it is the adiabatic approximation which permits bistability while we expect that the inclusion of memory effects suppresses it. We also conclude that bistable regimes induced by the electron-electron interaction only, are unlikely to be found in Hubbard or extended Hubbard model nanojunctions, and that other degrees of freedom, like molecular vibrations or nuclear coordinates, must be taken into account.

### Acknowledgments

Part of the calculations were performed at the CSC – IT Center for Science Ltd administered by the Ministry of Education, Science and Culture, Finland. A.S. acknowledges funding by the Academy of Finland under grant No. 140327/2010. S.K. acknowledges funding by the "Grupos Consolidados UPV/EHU del Gobierno Vasco" (IT-319-07). R.v.L. acknowledges the Academy of Finland for research funding under grant No. 127739. We acknowledge the support from the European Theoretical Spectroscopy Facility.

- 
- <sup>1</sup> V. J. Goldman, D. C. Tsui, and J. E. Cunningham, Phys. Rev. Lett. **58**, 1256, (1987).
- <sup>2</sup> J. O. Sofo and C. A. Balseiro, Phys. Rev. B **42**, 7292, (1990).
- <sup>3</sup> T. Fiig and A.-P. Jauho, Surface Science **267**, 392 (1992).
- <sup>4</sup> P. L. Pernas, F. Flores, and E. V. Anda, Phys. Rev. B **47**, 4779 (1993).
- <sup>5</sup> Z. Dai and J. Ni, Phys. Lett. A **342**, 272 (2005).
- <sup>6</sup> F. W. Sheard and G. A. Toombs, Appl. Phys. Lett. **52**, 1228 (1988).
- <sup>7</sup> A. Zaslavsky, V. J. Goldman, D. C. Tsui, and J. E. Cunningham, Appl. Phys. Lett. **53**, 1408 (1988).
- <sup>8</sup> N. Zou, M. Willander, I. Linnerud, U. Hanke, K. A. Chao, and Y. M. Galperin, Phys. Rev. B **49**, 2193 (1994).
- <sup>9</sup> C. Zhang, Appl. Phys. Lett. **78**, 4187 (2001).
- <sup>10</sup> A. A. Dzhioev and D. S. Kosov, J. Chem. Phys. **135**, 174111 (2011).
- <sup>11</sup> J. Chen, M. A. Reed, A. M. Rawlett, and J. M. Tour, Science **286**, 1550 (1999).
- <sup>12</sup> J. Chen and M. A. Reed, Chem. Phys. **281**, 127 (2002).
- <sup>13</sup> C. F. A. Negre, P. A. Gallay, and C. G. Sánchez, Chem. Phys. Lett. **460**, 220 (2008).
- <sup>14</sup> C. Sánchez, M. Stamenova, S. Sanvito, D.R. Bowler, A.P. Horsfield, and T. N. Todorov, J. Chem. Phys. **124**, 214708 (2006).
- <sup>15</sup> L. P. Kadanoff and G. Baym, *Quantum Statistical Mechanics* (Benjamin, New York, 1962).
- <sup>16</sup> N. E. Dahlen and R. van Leeuwen, Phys. Rev. Lett. **98**, 153004 (2007).
- <sup>17</sup> A. Stan, N. E. Dahlen, and R. van Leeuwen, J. Chem. Phys. **130**, 224101 (2009).
- <sup>18</sup> N. E. Dahlen, R. van Leeuwen, and A. Stan, J. Phys.: Conf. Ser. **35**, 340 (2006).
- <sup>19</sup> N. E. Dahlen, A. Stan, and R. van Leeuwen, J. Phys.: Conf. Ser. **35**, 324 (2006).
- <sup>20</sup> P. Myöhänen, A. Stan, G. Stefanucci, and R. van Leeuwen, Europhys. Lett. **84**, 67001 (2008).
- <sup>21</sup> P. Myöhänen, A. Stan, G. Stefanucci, and R. van Leeuwen, Phys. Rev. B **80**, 115107 (2009).
- <sup>22</sup> P. Myöhänen, A. Stan, G. Stefanucci, and R. van Leeuwen, J. Phys.: Conf. Ser. **220**, 012017 (2010).
- <sup>23</sup> G. Stefanucci and C.-O. Almbladh, Phys. Rev. B **69**, 195318 (2004).
- <sup>24</sup> R. Baer, T. Seideman, S. Ilani, and D. Neuhauser, J. Chem. Phys. **120**, 3387 (2004).
- <sup>25</sup> G. Stefanucci and C.-O. Almbladh, Europhys. Lett. **67**, 14 (2004).
- <sup>26</sup> S. Kurth, G. Stefanucci, C.-O. Almbladh, A. Rubio, and E. K. U. Gross, Phys. Rev. B **72**, 035308 (2005).
- <sup>27</sup> K. Burke, R. Car, and R. Gebauer, Phys. Rev. Lett. **94**, 146803 (2005).
- <sup>28</sup> X. Zheng, G. H. Chen, Y. Mo, S. K. Koo, H. Tian, C. Y. Yam, and Y. J. Yan, J. Chem. Phys. **133**, 114101 (2010).
- <sup>29</sup> C. Y. Yam, X. Zheng, G. H. Chen, Y. Wang, T. Frauenheim, and T. A. Niehaus, Phys. Rev. B **83**, 245448 (2011).
- <sup>30</sup> A.-M. Uimonen, E. Khosravi, G. Stefanucci, S. Kurth, R.

- van Leeuwen, and E. K. U. Gross, J. Phys.: Conf. Ser. **220**, 012018 (2010).
- <sup>31</sup> A.-M. Uimonen, E. Khosravi, A. Stan, G. Stefanucci, S. Kurth, R. van Leeuwen, and E. K. U. Gross, Phys. Rev. B **84**, 115103 (2011).
- <sup>32</sup> J. Jin, X. Zheng, and Y.J. Yan, J. Chem. Phys. **128**, 234703 (2008).
- <sup>33</sup> X. Zheng, J. Jin, S. Welack, M. Luo, and Y.J. Yan, J. Chem. Phys. **130**, 164708 (2009).
- <sup>34</sup> X. Zheng, J. Jin, and Y.J. Yan, New J. Phys. **10**, 093016 (2008).
- <sup>35</sup> F. Heidrich-Meisner, A. E. Feiguin, and E. Dagotto, Phys. Rev. B **79**, 235336 (2009).
- <sup>36</sup> G. Stefanucci, E. Perfetto, and M. Cini, Phys. Rev. B **81**, 115446 (2010).
- <sup>37</sup> I. V. Tokatly, Phys. Rev. B **83**, 035127 (2011).
- <sup>38</sup> P. Schmitteckert and F. Evers, Phys. Rev. Lett. **100**, 086401 (2008).
- <sup>39</sup> S. Schenk, P. Schwab, M. Dzierzawa, and U. Eckern, Phys. Rev. B **83**, 115128 (2011).
- <sup>40</sup> M. A. L. Marques, C. A. Ullrich, F. Nogueira, A. Rubio, K. Burke, and E. K. U. Gross, *Time-Dependent Density Functional Theory* Vol. 706 (Springer, Berlin, 2006).
- <sup>41</sup> N. A. Lima, M. F. Silva, L. N. Oliveira, and K. Capelle, Phys. Rev. Lett. **90**, 146402 (2003).
- <sup>42</sup> K. Schönhammer, O. Gunnarsson, and R.M. Noack, Phys. Rev. B **52**, 2504 (1995).
- <sup>43</sup> C. Verdozzi, Phys. Rev. Lett. **101**, 166401 (2008).
- <sup>44</sup> N. A. Lima, L. Oliveira, and K. Capelle, Europhys. Lett. **60**, 601 (2002).
- <sup>45</sup> S. Kurth, G. Stefanucci, E. Khosravi, C. Verdozzi, and E. K. U. Gross, Phys. Rev. Lett. **104**, 236801 (2010).
- <sup>46</sup> Y. A. Kuznetsov, *Elements of Applied Bifurcation Theory* (Springer-Verlag, New York, 1995).
- <sup>47</sup> L. V. Keldysh, Soviet Phys. JEPT **20**, 1018 (1965).
- <sup>48</sup> P. Danielewicz, Ann. Phys. (NY) **152**, 239 (1984).
- <sup>49</sup> R. van Leeuwen, N. E. Dahlen, G. Stefanucci, C.-O. Almbladh, and U. von Barth, Lect. Notes Phys. **706**, 33 (2006).
- <sup>50</sup> G. Baym, Phys. Rev. **127**, 1391 (1962).
- <sup>51</sup> G. Baym and L. P. Kadanoff, Phys. Rev. **124**, 287 (1961).
- <sup>52</sup> M. Puig von Friesen, C. Verdozzi, and C.-O. Almbladh, Phys. Rev. Lett. **103**, 176404 (2009).
- <sup>53</sup> Y. Meir and N. S. Wingreen, Phys. Rev. Lett. **68**, 2512 (1992).
- <sup>54</sup> G. Stefanucci, Phys. Rev. B **75**, 195115 (2007).
- <sup>55</sup> E. Khosravi, G. Stefanucci, S. Kurth, and E. K. U. Gross, Phys. Chem. Chem. Phys. **11**, 4535 (2009).
- <sup>56</sup> E. Khosravi, S. Kurth, G. Stefanucci, and E. K. U. Gross, Appl. Phys. A. **93**, 355 (2008).
- <sup>57</sup> K. S. Thygesen and A. Rubio, Phys. Rev. B **77**, 115333 (2008).